Post-print of: Yedra, L. et al. “Electron energy-loss spectroscopic tomography of $Fe_xCo_{(3-x)}O_4$ impregnated Co_3O_4 mesoporous particles: unravelling the chemical information in three dimensions” in Analyst (Ed. RSC), vol. 141, issue 16 (August 2016), p. 4968-4972. The final version is available at DOI 10.1039/C6AN00562D

Journal Name

ARTICLE

Electron Energy-Loss Spectroscopic Tomography of $Fe_xCo_{(3-x)}O_4$ Impregnated Co_3O_4Mesoporous Particles: Unraveling the Chemical Information in Three Dimensions

Received 00th January 20xx,
Accepted 00th January 20xx

DOI: 10.1039/x0xx00000x

www.rsc.org/

L. Yedra[a,b]†, A. Eljarrat[a], Raúl Arenal[c,d], L. López-Conesa[a], E. Pellicer[e], A. López-Ortega[f], M. Estrader[g], J. Sort[h], M. D. Baró[e], S. Estradé[a,b]and F. Peiró[a]

Electron energy-loss spectroscopy – spectrum image (EELS-SI) tomography is a powerful tool to investigate the three dimensional chemical configuration in nanostructures. Here, we demonstrate, for the first time, the possibility to characterize the spatial distribution of Fe and Co cations in a complex $Fe_xCo_{(3-x)}O_4/Co_3O_4$ ordered mesoporous system. This hybrid material is relevant because of the ferrimagnetic/antiferromagnetic coupling and high surface area. We unambiguously prove that the EELS-SI tomography shows a sufficiently high resolution to simultaneously unravel the pore structure and the chemical signal.

Introduction

Since the discovery of the first ordered mesoporous silica (OMS) in the early 1990s by the Mobil Oil Corporation[1], many different families of OMS have been synthesized and characterized. Their interest arises from the broad possibilities of tailoring the pore structure through the choice of surfactants, auxiliary chemicals and reaction conditions[2]. Due to the possibility to grow many different porous structures, these materials have been used as scaffolds for designing new high surface area framework materials (e.g. metals, metal oxides, semiconductors, carbons, nitrides). With a pore size of 2–50 nm, tunable pore topologies and extremely large surface areas, mesoporous materials hold a privileged position between microporous (e.g. zeolites) and macroporous materials. A number of metal oxides have been already grown inside the pores of OMS, followed by the selective removal of the parent OMS to release the metal oxide replica. This synthetic strategy is termed as nanocasting or hard-templating. The resulting replicas combine the physico-chemical properties of the metal oxide with the high surface area of the OMS. Applications of these materials range from photonics, electronics, gas sensing[3-5], fuel cell devices[6, 7] and catalysis[6, 8-13] to biomedical applications such as drug delivery, imaging or magnetic hyperthermia[14-18]. Importantly, while significant improvements in electron microscopy or small angle X-ray diffraction have permitted the accurate determination of the pore size of these materials, retrieving the three dimensional (3D) elemental composition mapping of the pore network still remains a challenge. The possibility to gather chemical information of the pore structure (not only of the utmost surface, but also of the inner pores) with high resolution constitutes a breakthrough. This information would be greatly appreciated in many fields. For instance, since porous materials are largely used in heterogeneous catalysis, one could exactly know the location of the most active sites of the catalyst materials. This would in turn open the possibility to synthesize on-demand novel porous frameworks with enhanced performance for the target application.

Electron energy loss spectroscopy (EELS) is an analytical technique centered on inelastic interactions between the electrons from the transmission electron microscope (TEM) and the sample. When travelling through the sample, the fast TEM electrons can transfer part of their energy to the electrons of the sample in a specific amount, related to different excitations of the sample electrons. A magnetic prism at the end of the TEM column deflects the electrons according to their energy, which, coupled with a CCD, gives us the EEL

[a] *Laboratory of ElectronNanoscopies (LENS)- MIND/IN2UB, Dept. d'Electrònica, Universitat de Barcelona, c/ MartíFranqués 1, E-08028 Barcelona, Spain.*
[b] *CCiT, Scientific and TechnologicalCenters, Universitat de Barcelona, E-08028, Barcelona, Spain.*
[c] *Laboratorio de Microscopias Avanzadas (LMA), Instituto de Nanociencia de Aragon (INA), Universidad de Zaragoza, E-50018 Zaragoza, Spain.*
[d] *Fundacion ARAID, E-50004 Zaragoza, Spain*
[e] *Departament de Física, Facultat de Ciències, UniversitatAutònoma de Barcelona, E-08193 Barcelona, Spain.*
[f] *INSTM and Dipartimento di Chimica “U. Schiff”, Universitàdegli Studi di Firenze, Via dellaLastruccia 3, Sesto Fiorentino, I-50019 Firenze, Italy*
[g] *Departament de Química Inorgànica, Universitat de Barcelona, Diagonal 645, E-08028, Barcelona, Spain.*
[h] *Institució Catalana de Recerca i EstudisAvançats (ICREA) and Departament de Física, Facultat de Ciències, UniversitatAutònoma de Barcelona, E-08193 Barcelona, Spain.*

† E-mail: *lluis.yedra@el.ub.edu*
Present Address: Luxembourg Institute of Science and Technology (LIST), 41, rue du Brill, L-4422 Belvaux, Luxembourg.

Electronic Supplementary Information (ESI) available: Description of the material preparation, data acquisition and MVA data treatment (PDF). Movie of the 3D chemical information (MPG).

spectrum, where the abscise axis corresponds to the amount of lost energy and the ordinate axis to the counts (i.e., the number of electrons having lost that amount of energy). Compared to energy dispersive x-ray spectroscopy (EDS), EELS offers a slightly higher spatial resolution, as transmitted electrons are less sensitive to broadening effects, but its main advantage over EDS for tomography is the higher and constant collection efficiency throughout the experiment[19].Using EELS in the TEM, chemical, electronic and structural information can be extracted. Recently, the suitability of EELS spectrum imaging (EELS-SI)[20-22] as a signal for tomographic reconstruction of ordered mesoporous silica (OMS) matrices has been demonstrated[23]. Its main advantage over the more expanded energy filtered transmission electron microscopy (EFTEM)[24-27] technique is that EELS-SI retains fine chemical and electronic sensitivity in a wider energy range. Notably, this information can be reconstructed in 3D, thus rendering 3D chemical information at the nanoscale. EELS-SI tomography consists in acquiring a series of spectrum images at different tilt angles, analogously to most of the tomographic techniques in the TEM. Afterwards, the information contained in the spectra must be extracted for reconstruction. The extracted signals must fulfill the projection requirement[28], which states that any information suitable for tomographic reconstruction must be a monotonic function of some property of the sample.

In the present work we demonstrate that EELS tomography is capable of reconstructing the 3D long-range order packing of mesopores while offering a unique chemical insight to the heterostructured material, down to the pore resolution (i.e., truly at the nanoscale). Principal component analysis (PCA), a form of multivariate statistical analysis (MVA) is used to reduce the noise of the dataset, therefore enabling short acquisition times, and the intensities of the EELS edges are used for 3D reconstruction. As already mentioned, we have applied this technique to nanocast Co_3O_4mesoporous particles (obtained from KIT-6 silica) subsequently impregnated with iron (III) nitrate precursor in order to form a $Fe_xCo_{(3-x)}O_4$ shell coating the Co_3O_4 mesopores[29]. The interest of this bi-magnetic system arises from the enhanced exchange bias that results from the coupling between the antiferromagnetic (AFM) Co_3O_4 and the ferrimagnetic (FiM) $Fe_xCo_{(3-x)}O_4$. The present experiment was aimed at providing a clear-cut answer to an open question; whether the synthesized nanocomposite material consisted of a simple $Fe_xCo_{(3-x)}O_4$ coating of the utmost surface of the Co_3O_4 particles (case i) or if a mixed phase of cobalt and iron oxides (i.e., $Fe_xCo_{(3-x)}O_4$ phase) had been formed at the inner pores of the Co_3O_4 host (case ii). EELS-tomography is shown to be capable of answering this question. The existence of a 3D core-shell structure (case ii) is confirmed, hence making EELS-tomography a unique tool in nanostructure characterization.

Results

A total of 36 EELS-SI, 63x63 spectra each, were acquired between -64° and 72°. Due to the low electron beam voltage (80 kV) and short acquisition times (200 ms per pixel) used to avoid sample damage during such a long experiment, the data sets happened to be very noisy. As in previous works[23], multivariate analysis (MVA) in Hyperspy[30] was efficiently applied to separate most of the noise from the signal information in the EELS-SI.

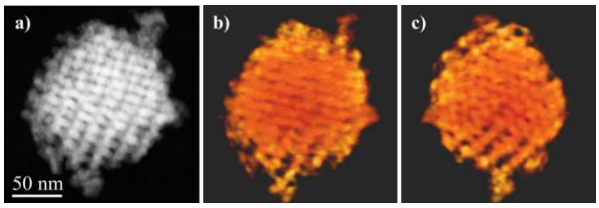

Figure 1. a) High-angle annular dark field (HAADF) image acquired at -4°, half through the acquisition series. b) and c) views of the 3D reconstruction of the HAADF images. The porous structure is preserved in the 3D model.

Raw and noise reduced spectrum images are shown in Figures 2a and 2c, respectively. After noise reduction, the images were thresholded to eliminate the spurious intensities in areas outside the particle. Raw and noise reduced spectra, corresponding to the sum of four individual spectra in a point of the SI are presented in Figure 2b and 2d, respectively. MVA accurately extracts the actual information contained in the data, as it is observed in the spectrum from the same area after the statistic data treatment.

From this clean dataset the elemental edge intensity can be calculated, through background removal and integration of the areas under the oxygen K, iron $L_{2,3}$ and cobalt $L_{2,3}$ edges, as illustrated in Figure 3a. As a result, individual maps of the three elements plus an image using the background before the oxygen edge could be obtained for every tilt angle, as presented in Figures 3b-3e corresponding to the first SI acquisition at -4°). These four sets of signal maps are suitable for 3D reconstruction since, to a first approximation, the background before the O edge is only proportional to the thickness of the sample and the integrated area under the edges is proportional to the thickness and the concentration of a given element, so fulfilling the projection requirement. These four signals were successfully reconstructed in 3D, as shown in Figure 4. However, they do not have the same spatial resolution. Taking into account the definition of the inner pores as the main feature to be preserved in the reconstruction, the background signal yields the best spatial resolution. This is observed in Figure 3b where the pores of the structure are resolved all over the particle. If we compare the different elemental signal maps extracted also from this -4° orientation, iron (Figure 3d) and cobalt (Figure 3e) (maps show defined pores all over this projection. Only at the centre of the particle does the pore structure appear more blurred. On the other hand, oxygen signal (Figure 3c) is only accurate at the border of the particle, so the pore structure is not visible inside the particle.

The four sets of signal maps were successfully reconstructed in 3D, as shown in Figure 4. Concerning the resolution of the pores after 3D reconstructions, cobalt (Figure 4c and 4g) and iron (Figure 4d and 4h) reconstructions yield a visible porous structure while this is not the case for the oxygen signal (Figure 4b and 4f). However the oxygen signal can reconstruct the

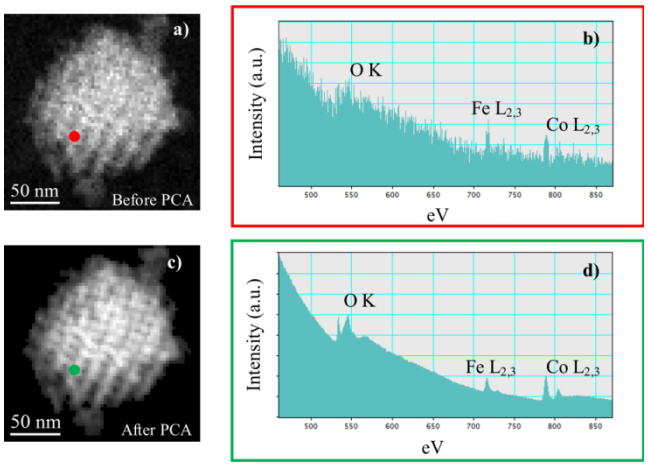

Figure 2. a) SI at -4° as acquired. b) EELS spectrum corresponding to the sum of 4 spectra in the region highlighted in (a). c) SI at -4° after PCA noise reduction. d) EELS spectrum corresponding to the sum of 4 spectra in the region highlighted in (c). The noise was reduced not only in the spectrum but also in the images.

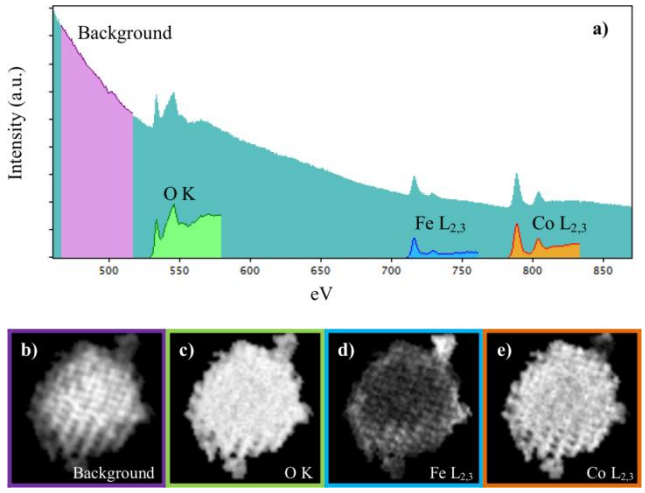

Figure 3. a) Single spectrum from the clean dataset at -4° tilt, where the shaded areas correspond to the integrated intensities of the pre-O K background and O K, Fe $L_{2,3}$ and $CoL_{2,3}$ edges. Extracted intensities from the SI, for a tilt angle of -4°, for the pre-O K background (b), the oxygen K edge (c), the Fe $L_{2,3}$ edge (d) and the cobalt $L_{2,3}$ edge (e), respectively.

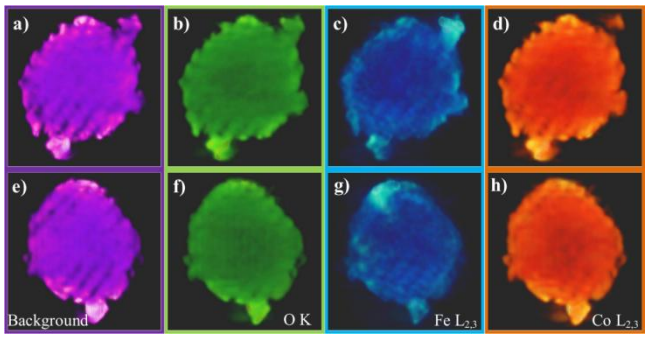

Figure 4. Voltex visualizations of the reconstructed volume for the extracted intensities of the background (a) and e)), O K edge (b) and f)), Fe $L_{2,3}$ edge (c) and g)) and Co $L_{2,3}$ edge (d) and h)). See the supporting information for the animated version.

porous structure at the border, as clearly observed in Figure 4b and Figure 4f.

Iron and cobalt signals reconstruct the porous structure with good accuracy. The 3D reconstruction revealed two protuberances on the particle surface, one of them having a different composition from the rest of the sample. From Figure 3 and Figure 4, it is evident that the topmost protuberance is iron-rich while the bottom one has the same mean composition as the rest of the sample. This is also noticed in Figure 5, where Fe (in blue) and Co (in orange) reconstructions are superimposed. This figure also shows how the pores of the mesoporous cobalt oxide template have been successfully impregnated with the mixed iron-cobalt oxide, as the signal from iron (in blue) is nicely seen inside the mesoporous structure. This observation is confirmed in Figure 6, where the covering of the cobalt oxide structure with iron is shown in a slice through the reconstructed volume. Thus, in this case, we could obtain the information from inside the nanoparticle. It is important to note that this technique is the only one providing such significant information about the intimate chemical configuration at this spatial resolution.

Discussion

The suitability of the technique must be discussed in terms of the projection requirement, which states that, in order to be reconstructed, a signal must be a monotonous function of some property of the material. Signals failing this requirement have strong streaking artefacts (brighter or darker lines spanning the whole volume, including sample and vacuum) that impeach the intensities in the back-projection reconstruction to have any physical link with the actual sample.

The extracted intensity under the EELS edges can be expressed in the form

$$I_k^A(\beta,\Delta) = N^A \sigma_k^A(\beta,\Delta) I_0 \qquad (1)$$

where I_k^A is the edge intensity of a k transition for an element *A*, integrated over an angle β, the collection angle of the spectrometer, and in the energy range Δ, N^A is the areal density of element *A* (concentration times thickness), σ_k^A is the k ionization partial cross-section of element *A* and I_0 is the zero loss intensity.

If our particles were thin enough for one single scattering event to take place, the signal under a given edge would only be proportional to the I_k^A thickness and the concentration of a given element. The effects of plural scattering are avoided for thicknesses (t) of the sample $t/\lambda \leq 0.3$[19], where λ is the inelastic scattering mean free path. The thickness of the particle is around 100 nm (as seen in Figure 1) and the ionization mean free path is around 80 nm. Therefore, plural scattering can be expected. It has already been proposed that the EELS signal can still behave monotonically while t/λ<2 [24] and be reconstructed. In our case we do observe a slight loss of intensity of the signal towards the centre of the particle. However, we can still qualitatively interpret the distribution of the elements in the reconstruction. Also, the increased

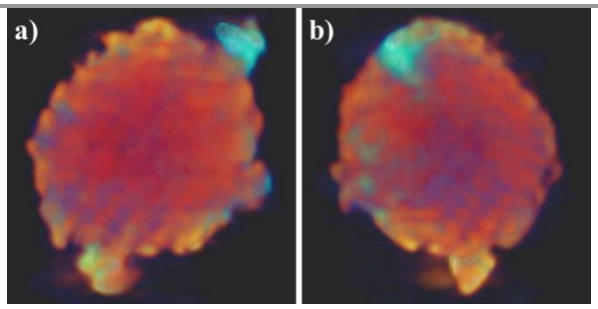

Figure 5. Comparison of cobalt (orange) and iron (blue) reconstructions in two different orientations of the reconstructed volumes, where the presence of iron inside the pores can be resolved.

thickness close to the centre results in a loss of spatial resolution for all the integrated edge signals. This is visible in the reconstructed signals in Figure 4 as well as in Figure 6b. The porous structure is difficult to recognise in these parts, which still preserve the information that the iron is distributed homogeneously and has reached all the inner porous channels and has not remained just on the surface. The actual distribution of iron with respect to cobalt appears more clearly in the pores in thinner areas. In this case, the information offered by the background signal has been important for the interpretation.

As far as the background signal is concerned, we can assume that the background before the O K edge is only caused by the tail of the low loss region, dominated by the bulk plasmon. After this edge, the background has a significant contribution of the Bethe ridge onto the plasmon. The bulk plasmon is a collective oscillation of electrons in the valence band. Cobalt and iron are consecutive elements and their oxides present in this sample are both spinels with similar unit cell size. Therefore, the new material grown on top of the original cobalt oxide structure, either iron-cobalt mixed oxide or iron oxide, grows epitaxially. As a result, the plasmons in our sample can be considered independent of the compositional changes. In this case, only the thickness of the material is involved in the intensity of the plasmon and, thus, in the intensity of the background prior to the first core loss edge. In other words, the pre-O K edge background signal can be interpreted as a measure of thickness.

Coming back to the main point, the distribution of iron and cobalt, by only observing figures 5 and 6b, it might appear that the pores in the cobalt structure are clogged with iron. However, the thickness maps from the background signal in Figure 6a do clearly show that there is still a remaining pore structure. The clogged appearance can be explained as an artefact from the delocalisation of the chemical signals in the reconstruction process. We can use the measured pore structure (figure 6c) in the reconstruction to estimate its resolution. Using the background, 5 nm separated peaks could be measured. In the Fe and Co maps, we can use the half distance between the peaks, which is around 9 nm. These values depend on the resolution of the original images and, therefore, leave space for further improvement of the technique, only limited by EELS-SI resolution. While it can reach the atomic column level, there has to be a trade of

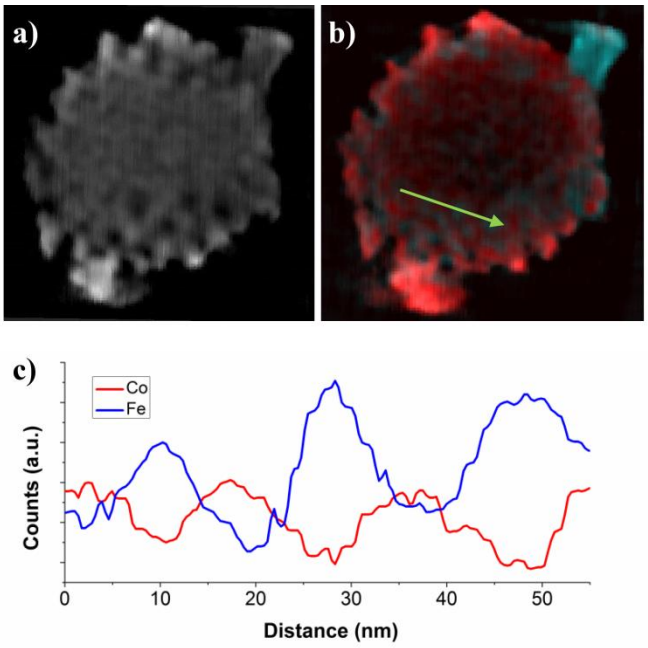

Figure 6. a) Slice through the reconstructed volume of the background signal and b) compositional map of the slice from cobalt (red) and iron (blue) signals. It can be observed how the inner sides of the pores are iron-rich, as expected from the infiltration procedure. This is further observed in the linescan (c) along the green arrow in b)

resolution if the sample is sensitive to the beam, due to the multiple images needed for tomography. To sum up, EELS-SI tomography has allowed us to confirm that the desired core-shell AFM-FiM structure is obtained (Figure6). This technique has yielded 3D reconstructions of the particle using chemical sensitive signals, therefore obtaining 3D representations of the elemental distribution in the sample. In these 3D representations, the presence of iron covering the inner pores is demonstrated, and, most importantly, it is possible to extract much localized chemical information from the interior of the particle, confirming the expected structure.

Conclusions

EELS-SI tomography offers a novel way to disentangle the 3D chemical composition of nanostructured materials. In this study $Fe_xCo_{(3-x)}O_4$@Co_3O_4mesoporous particles have been successfully reconstructed in 4D, with chemical composition being the 4th dimension, added to the 3 dimensions of the tomographically reconstructed volume. Thanks to the enhanced spatial resolution obtained even at low voltages (80 kV) using a probe aberration corrected instrument, and the ability of multivariate analysis to extract useful information from noisy data, it has been possible to unambiguously prove that the $Fe_xCo_{(3-x)}$ does coat the inner pores of the Co_3O_4 template, thus rendering a core-shell nanocomposite 3D structure.

Acknowledgements

The TEM measurements were performed in the Laboratorio de MicroscopiasAvanzadas (LMA) at the Instituto de Nanociencia de Aragon (INA) - Universidad de Zaragoza (Spain). The research leading to these results has received funding from the European Union Seventh Framework Program under Grant Agreement 312483 - ESTEEM2 (Integrated Infrastructure Initiative – I3) and the Spanish CSD2009-00013 and MAT2013-41506 research projects. Catalan government funding from 2014-SGR-1015 and 2014-SGR-672 research projects is also appreciated. R.A. acknowledges funding from MINECO-Spain (FIS2013-46159-C3-3-P). E.P. is grateful to MINECO for the 'Ramón y Cajal' contract. M.E. acknowledges the Spanish Ministry of Science and Innovation through the Juan de la Cierva Program. Partial funding from the European Research Council (Consolidator Grant, project nº 648454, SPIN-PORICS) is acknowledged.

Notes and references

1 C. Kresge, M. Leonowicz, W. Roth, Vartuli, and J. Beck, *Nature* 1992*,* **359**, 710.
2 J. Beck, J. Vartuli, W. Roth, M. Leonowicz, C. Kresge, K. Schmitt, C. Chu, D. Olson, E. Sheppard, S. McCullen, J. Higgins and J. Schlenker,. *J. Am. Chem. Soc.,* 1992*,* **114**, 10834.
3 E. Rossinyol, A. Prim, E. Pellicer, J. Arbiol, F. Hernández-Ramírez, F. Peiró, A. Cornet, J.R. Morante, L.A. Solovyov, B. Tian, T. Bo and D. Zhao,. *Adv. Funct. Mat.,* 2007*,* **17**, 1801.
4 A. Prim, E. Pellicer, E. Rossinyol, F. Peiró, A. Cornet and J.R. Morante, *Adv. Funct. Mat.,* 2007*,* **17***,* 2957.
5 L. Francioso, A. Forleo, S. Capone, M. Epifani, A. Taurino and P. Siciliano, *Sens. Actuator B-Chem.,* 2006*,* **114**, 646.
6 E. Rossinyol, E. Pellicer, A. Prim, S. Estrade, J. Arbiol, F. Peiro, A. Cornet, J.R. Morante, *J Nanopart. Res.,* 2008*,* **10**, 369.
7 M. Cabo, S. Garroni, E. Pellicer, C. Milanese, A. Girella, A. Marini, E. Rossinyol, S. Surinach and M.D. DolorsBaro,. *Int. J. Hydrogen Energ.,*2011*,* **36**, 5400.
8 B. Sahoo, S.K. Sahu, S. Nayak, D. Dhara and P Pramanik, *Catal. Sci. Technol.,* 2012*,* **2**, 1367.
9 B.Y. Song, Y. Eom, and T.G. Lee,*Appl. Surf. Sci.,* 2011*,* **257**, 4754.
10 S. Tao, C. Wang, W. Ma, S. Wu and C. Meng, *MicroporousMesoporous Mater.,* 2012*,* **147**, 295.
11 I. Ursachi, A. Stancu, and A. Vasile,.*J. Colloid Interface Sci.,* 2012*,* **377**, 184.
12 Y. Wang, B. Li, L. Zhang, P. Li, L. Wang and J Zhang, *Langmuir,* 2012*,* **28**, 1657.
13 C. Yuan, Z. Huang and J. Chen, *Catal. Lett.,*2011*,* **141**, 1484.
14 Y. Chen, H. Chen, S. Zhang, F. Chen, S. Sun, Q. He, M. Ma, X. Wang, H. Wu, L. Zhang, L. Zhang and J. Shi, *Biomaterials,* 2012*,* **33**, 2388.
15 M. Ma, H. Chen, Y. Chen, X. Wang, F. Chen, X. Cui and J. Shi, *Biomaterials* **2012***, 33*, 989.
16 H. Wu, L. Tang, L. An, X. Wang, H. Zhang, J. Shi and S. Yang, *React. Funct. Polym.,*2012*,* **72**, 329.
17 M. Liong, J. Lu, M. Kovochich, T. Xia, S.G. Ruehm, A.E. Nel and J.I. Zink, *ACS nano,* 2008, **2**, 889.
18 S. Gai, P. Yang, C. Li, W. Wang, Y. Dai, N. Niu and J. Lin, *Adv. Funct. Mat.,* 2010, **20***,* 1166.
19 R.F. Egerton, Plenum Press: New York,1996.
20 K. Jarausch, P. Thomas, D.N. Leonard, R. Twesten and C.R. Booth, *Ultram.,* 2009*,* **109**, 326.
21 B. Goris, S. Turner, S. Bals and G. Van Tendeloo, *ACS nano* 2014 doi:10.1021/nn5047053
22 G. Haberfehlner, A. Orthacker, M. Albu, J. Li and G. Kothleitner, *Nanoscale*2014. doi:10.1039/C4NR04553J
23 L. Yedra, A. Eljarrat, R. Arenal, E. Pellicer, M. Cabo, A. Lopez-Ortega, M. Estrader, J. Sort, M.D. Baró, S. Estradéand F. Peiró, *Ultram.,*2012*,* **122**, 12.
24 G. Möbus, R.C. Doole and B.J. Inkson, *Ultram.,*2003*,* **96**, 433.
25 M. Weyland and P.A. Midgley, *Microsc. Microanal.,*2003*,* **9**, 542.
26 R.D. Leapman, E. Kocsis, G. Zhang, T.L. Talbot and P. Laquerriere, *Ultram.* 2004*,* **100**, 115.
27 I. Florea, O. Ersen, R. Arenal, D. Ihiawakrim, C. Messaoudi, K. Chizari, I. Janowska and C. Pham-Huu, *J. Amer. Chem. Soc.,* 2012, **134**, 9672.
28 P.W. Hawkes, The Electron Microscope as a Structure Projector, 2006, 83.
29 E. Pellicer, M. Cabo, A. Lopez-Ortega, M. Estrader, L. Yedra, S. Estradé, F. Peiró, Z. Saghi, P. Midgley, E. Rossinyol, I.V. Golosovsky, A. Mayoral, J.D. Prades, S. Surinach, M.D. Baró, J. Sort and J. Nogués, *Nanoscale,* 2013*,* **5**, 5561.
30 R. Arenal, F. De la Pena, O. Stephan, M. Walls, M. Tence, A. Loiseau and C. Colliex, *Ultram*., 2008, **109**, 32.